JACS
JOURNAL OF THE AMERICAN CHEMICAL SOCIETY
Article
pubs.acs.org/JACS

Performance Improvement of Nanocatalysts by Promoter-Induced Defects in the Support Material: Methanol Synthesis over Cu/ZnO:Al

Malte Behrens,*[,†] Stefan Zander,[†] Patrick Kurr,[‡] Nikolas Jacobsen,[‡] Jürgen Senker,[§] Gregor Koch,[∥] Thorsten Ressler,[∥] Richard W. Fischer,[⊥] and Robert Schlögl[†]

[†]Department of Inorganic Chemistry, Fritz-Haber-Institut der Max-Planck-Gesellschaft, Faradayweg 4-6, 14195 Berlin, Germany
[‡]Clariant Produkte (Deutschland) GmbH, BU Catalysts, Waldheimer Str. 13, 83052 Bruckmühl, Germany
[§]Inorganic Chemistry III, University of Bayreuth, Universitätsstr. 30, 95447 Bayreuth, Germany
[∥]Institut für Anorganische und Analytische Chemie, Technische Universität Berlin, Straße Des 17. Juni 135, 10623 Berlin, Germany
[⊥]Lehrstuhl I für Technische Chemie, Technische Universität München, Lichtenbergstr. 4, 85747 Garching, Germany

Supporting Information

ABSTRACT: Addition of small amounts of promoters to solid catalysts can cause pronounced improvement in the catalytic properties. For the complex catalysts employed in industrial processes, the fate and mode of operation of promoters is often not well understood, which hinders a more rational optimization of these important materials. Herein we show for the example of the industrial $Cu/ZnO/Al_2O_3$ catalyst for methanol synthesis how structure−performance relationships can deliver such insights and shed light on the role of the Al promoter in this system. We were able to discriminate a structural effect and an electronic promoting effect, identify the relevant Al species as a dopant in ZnO, and determine the optimal Al content of improved Cu/ZnO:Al catalysts. By analogy to Ga- and Cr-promoted samples, we conclude that there is a general effect of promoter-induced defects in ZnO on the metal−support interactions and propose the relevance of this promotion mechanism for other metal/oxide catalysts also.

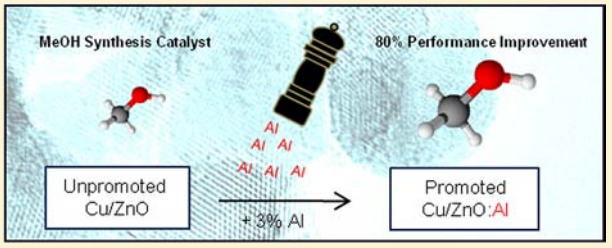

INTRODUCTION

Promotion of a heterogeneous catalyst (i.e., adding small amounts of one or more extra elements to a proven catalytic system) can have a huge impact on the catalytic properties,[1,2] and most industrially applied catalysts are somehow promoted. The final formulation of state-of-the-art catalysts often is a result of long-standing, mostly empirical optimization to improve the catalytic activity, selectivity, and stability. While model catalysis is powerful for understanding the intrinsic catalytic properties of the active phase and in many cases also for studying its interaction with the support,[3−5] detailed insight into the nature of the extrinsic effects of promoter species in powder catalysts is often lacking. Instead, promotion is often done in a rather specific and phenomenological manner, and more understanding as well as generic concepts for a more rational application of catalyst promoters is highly desirable.[1]

There are two categories of promoters that can be differentiated by means of their effect on the catalyst, so-called structural and electronic promoters.[2] The former usually increases the number of active sites and stabilizes the active phase in a highly dispersed state by improving the textural properties of the material. The latter affects the nature of the active sites by changing the bonding properties of surface adsorbates. Important examples where model studies have contributed a great deal of understanding of the promoting effect of such bonding modifiers involve alkali promoters added to metal catalysts. For instance, K was found to have a beneficial effect on the selectivity of steam reforming of methane by increasing the energy barrier of methane dissociation and thus suppressing formation of carbonaceous deposits.[6] Another example is ammonia synthesis on Fe-based catalysts, where addition of K adatoms leads to an increase in the sticking coefficient of nitrogen, which has an accelerating effect on ammonia formation.[7]

The Al_2O_3-promoted Cu/ZnO catalyst system is employed in the industrial synthesis of methanol from $H_2/CO_2/CO$ mixtures (syngas) at approximately 60 bar and 250 °C. The catalyst is also active in steam reforming of methanol and the (reverse) water gas shift reaction. In the low-temperature forward shift reaction, Cs can act as an electronic promoter.[8]

In addition to enduring industrial relevance, there currently is renewed interest in such conversions of C1 molecules and the role of the promoting oxide[9,10] because of their potential for chemical storage and distribution of hydrogen and chemical fixation of CO_2.[11,12] Methanol has been proposed as a sustainable synthetic fuel if regenerative hydrogen and anthropogenic CO_2 are used for its synthesis.[13] These attractive new fields of application require continuous optimization of the

Received: October 23, 2012
Published: March 14, 2013

dx.doi.org/10.1021/ja310456f | J. Am. Chem. Soc. 2013, 135, 6061−6068

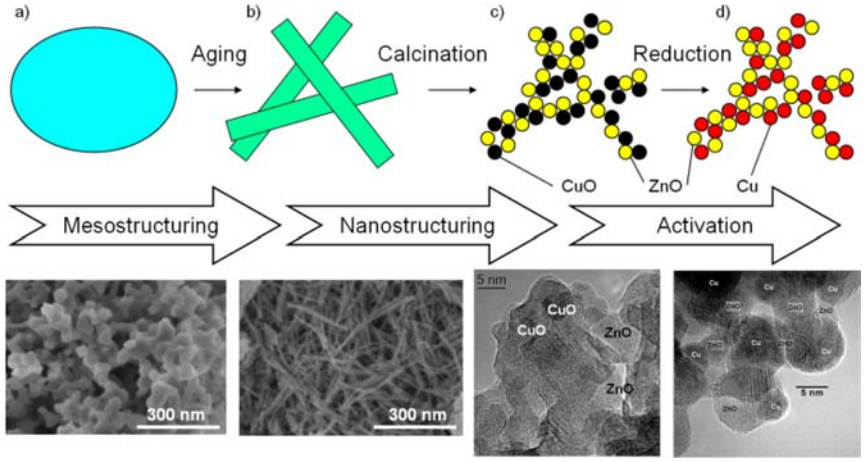

Figure 1. Simplified preparation scheme for the Cu/ZnO catalyst and electron microscopy images of the different stages of preparation. Upon aging in the mother liquor, the initial coprecipitate (a) yields zincian malachite (zM) (b). Under optimized conditions, zM is obtained in the form of thin needles with large interparticle pores. During calcination, the individual needles of zM undergo thermal decomposition, yielding an intimate mixture of CuO and ZnO (c). Better interdispersion of these two phases is achieved when a greater amount of Zn is incorporated into zM to dilute the Cu ions. Finally, the CuO component is reduced in hydrogen, yielding nanoparticulate Cu/ZnO with a unique microstructure exhibiting high porosity and high Cu dispersion. (Figure adopted from previous work[17]).

catalyst system to improve its performance when operated with nonfossil feed gas (e.g., with a varying $CO:CO_2$ ratio).

The $Cu/ZnO/Al_2O_3$ system has been widely studied for over 40 years in industry, mostly for applications in industrial methanol synthesis,[14] and also in academia for methanol steam reforming, but there are still many open questions concerning its mode of operation, including the mechanism of promotion. Highly active catalysts contain porous aggregates of strained[15] Cu metal particles stabilized by ZnO nanoparticles (Figure 1d) and exhibit a molar Cu:Zn ratio near 70:30.[16,17] This unique porous microstructure can be achieved through coprecipitation[18] and thermal treatment[19] of a mixed hydroxycarbonate precursor[20] (Figure 1a,b).

It is well-known that the addition of Al improves the performance of the binary Cu/ZnO catalyst and acts as a structural promoter.[21,22] A significant increase in methanol synthesis activity and thermal stability of the catalyst upon addition of Al_2O_3 (typically 5−10 mol % based on metal) to the Cu/ZnO system has been reported. The nature of this promoting effect as well as the speciation of Al in the final catalyst is, however, only poorly understood, which hinders knowledge-based optimization of Cu/ZnO-based catalysts for new energy-related applications. The promoter is thought to play a key role in the catalyst developed for syngas conversion operating in pure CO_2/H_2 feeds.[23] In the following, we first present a detailed study of the effectiveness of promoter incorporation during the technically applied catalyst synthesis and subsequently report on the fate of the promoter during catalyst activation and relate the results to the performance data.

EXPERIMENTAL SECTION

The precursor materials were prepared by coprecipitation from copper(II)/zinc nitrate solutions (70:30) acidified with nitric acid. Appropriate amounts of aluminum nitrate were added to obtain Al contents (i.e., [Al]/{[Cu] + [Zn] + [Al]}) of 0, 2.5, 3.3, 4.0, 6.5, and 13 mol %. Analogous Ga- or Cr-promoted samples were prepared with 1, 2, 2.5, 3, and 3.5 mol % Ga or Cr. Coprecipitation was performed using sodium carbonate solution as the precipitating agent at constant pH of 6.5 and T = 65 °C in an automated laboratory reactor. The precipitate was aged in the mother liquor at the same temperature until approximately 30 min after a minimum in pH (a maximum in turbidity) was observed, indicating the crystallization of zM.[17] Mg-modified Cu/ZnO was prepared similarly but at pH 9 with 0, 3, and 5 mol % Mg. Turbidity and pH logs during the aging period of the Al-promoted samples are shown in Figure S1 in the Supporting Information. The precursors were calcined in static air at 330 °C (2 °C/min) in a muffle furnace.

Powder X-ray diffraction (PXRD) patterns were recorded on a STOE Stadi-P diffractometer equipped with a primary focusing Ge monochromator (Cu $K\alpha_1$ radiation) and a linear-position-sensitive detector (moving mode, step size 0.1°, counting time 10 s/step, resolution 0.01°, total accumulation time 634 s). The samples were mounted in the form of a clamped sandwich of small amounts of powder fixed with a small amount of grease between two layers of thin polyacetate film. Pattern fitting and phase analysis were carried out using the Rietveld method as implemented in the TOPAS software package.[24] The amorphous fraction of the catalyst precursors was estimated using the Rietveld spiking method with NIST-certified ZnO as an internal standard and found to be low (for details, see the Supporting Information).

For the NMR experiments, the samples were reduced in 5% H_2 in Ar at 250 °C (2 K/min) for 30 min in a fixed-bed reactor (CE Instruments TPDR/O 1100) and transferred without further contact to air. High-resolution ^{27}Al solid-state NMR spectra were collected with a Bruker Avance II 300 spectrometer operating at 7.05 T with a resonance frequency of 78.2 MHz using a 4 mm triple-resonance magic-angle-spinning (MAS) probe. The shifts were referenced to $AlCl_3$ in an acidic aqueous solution. To eliminate unwanted contributions from the probe, all of the spectra were measured using three back-to-back $\pi/8$ pulses with a duration of 2 μs each and 18 432 repetitions.[25] The spinning speed was set to 12 kHz, and a recycle delay of 1.5 s ensured the total rebuild of the polarization before each scan.

Ga K-edge X-ray absorption near-edge structure (XANES) spectra were recorded at the X beamline at HASYLAB at DESY (Hamburg, Germany). Samples were measured in transmission mode over the range 9570−10580 eV to include the Ga K-edge at 10367 eV and the Zn K-edge at 9659 eV. Simultaneously, measurements on a Zn foil were conducted for spectrum calibration. The catalyst samples and Zn-containing references were prepared by diluting 30 mg of sample with 90 mg of polyethylene. In case of pure Ga_2O_3 references, 12 mg of sample were diluted with 88 mg of polyethylene. These mixtures were pressed to 13 mm diameter pellets with a force of 0.5 t for 30 s. Data analysis was performed using the Athena software package. Energy

dx.doi.org/10.1021/ja310456f | J. Am. Chem. Soc. 2013, 135, 6061−6068

calibration, background subtraction, and normalization were performed before reference spectra were fitted to the catalyst spectrum. Further XRD results and TGA data are shown in Figures S2 and S3, respectively, in the Supporting Information.

Specific Cu surface areas were determined using N_2O reactive frontal chromatography[32] at room temperature[33] in a fixed-bed reactor coupled to a mass spectrometer (1% N_2O in He, 80 mL/min). Catalytic testing in methanol synthesis was performed using an eight-channel parallel fixed-bed reactor setup working at 60 bar with a syngas mixture (59.5% H_2, 8.0% CO_2, 6.0% CO, remainder inert). Gas chromatography was used for exhaust gas analytics. Each passivated catalyst sample (170 mg) was loaded into the reactor, and the surface was reduced prior to the measurement in diluted hydrogen at 250 °C at ambient pressure. After conversion was stable at 250 °C, the catalytic activity was measured for 12 h. The reaction temperature was then lowered to 210 °C, and the performance was measured again for 12 h. The maximal approaches to equilibrium were 6% for CO conversion at 210 °C and 42% for CO_2 conversion.

RESULTS AND DISCUSSION

For this study, we varied the concentration of Al^{3+} ([Al]) in the mixed copper(II)/zinc/aluminum nitrate solution used for coprecipitation of the catalyst precursor (for details, see Figure S1 in the Supporting Information). The Cu:Zn ratio was fixed to 70:30 in all of the samples, and the highest Al content was [Al] = 13 mol % (metal-based), representing a typical composition of a state-of-the-art industrially employed system.[26] From there, [Al] was lowered while all other synthesis conditions were kept constant. The precipitated precursors were transformed into active catalysts following the multistep procedure outlined in Figure 1, which represents the applied manufacture of industrial methanol synthesis catalysts first introduced by ICI in the 1960s.[20]

The catalytic activity in the synthesis of methanol for this series of catalysts (expressed as the methanol yield normalized to the yield obtained using unpromoted binary Cu/ZnO catalyst) as a function of Al content is shown in Figure 2a (closed symbols). Comparison of the end members of the series (binary Cu/ZnO and the state-of-the-art catalyst containing 13% Al) shows an activity increase of 25% as a result of promotion with Al_2O_3. This result is in good agreement with literature data.[22] Interestingly, for intermediate promoter concentrations, the activity did not show a steady trend but instead exhibited a rather sharp maximum near [Al] = 3−4%. The activity of the most active sample, which contained 3.3% Al, was 143% relative to the 13% Al sample and 179% relative to the binary catalyst. These large differences in activity are surprising considering the relatively small differences in total composition, especially in the range 0% ≤ [Al] ≤ 6.5%. An explanation was found by structural analysis of the coprecipitated precursor material.

The importance of the coprecipitated hydroxycarbonate precursor for the performance of the resulting Cu/ZnO/(Al_2O_3) catalyst has been shown in many studies.[17,18,20,27−29] Upon aging of the coprecipitate, the crystalline precursor compound zincian machite (zM), $(Cu,Zn)_2(OH)_2CO_3$, is formed (Figure 1a,b). In this important precursor phase, the Cu dispersion of the final catalyst is already predetermined: The greater the extent of Cu^{2+} "dilution" by Zn^{2+} in the zM lattice, the higher will be the Cu dispersion in the final catalyst. Thus, the crystallization conditions and the degree of Zn^{2+} incorporation in zM are crucial for the activity of the Cu/ZnO catalyst because of the geometrical nanostructuring effect, as shown schematically in Figure 1.

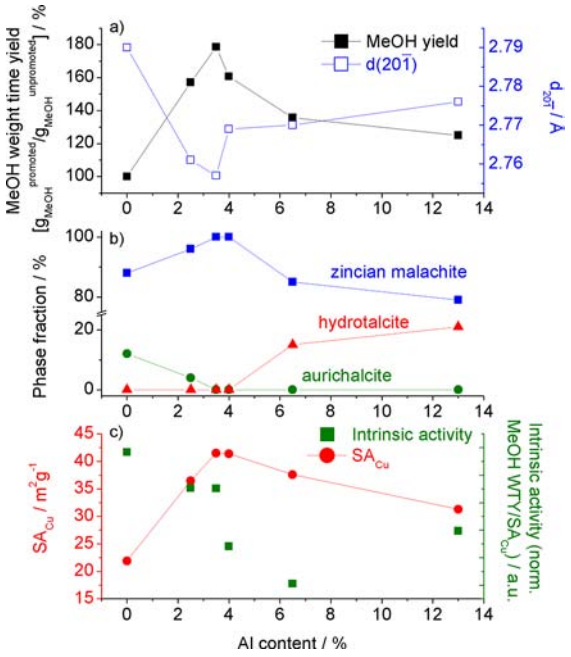

Figure 2. (a) $d_{20\bar{1}}$ spacing of the zM precursor (blue) as a measure of Zn incorporation (see the text) and performance of the resulting catalysts (black) in methanol synthesis as functions of Al promoter content. (b) Phase fractions in the precursor material. (c) Cu surface area and intrinsic activity of the Cu/ZnO/Al_2O_3 catalysts.

The phase composition of the precursor materials was evaluated by Rietveld refinement of the PXRD data (Figure S4 in the Supporting Information). All of the samples in this study contained zM as the major phase (Figure 2b). At [Al] = 13.0%, an additional hydrotalcite-like byproduct phase, $(Cu,Zn)_xAl_{1-x}(OH)_2(CO_3)_{x/2}\cdot mH_2O$, was found, whereas aurichalcite, $(Cu,Zn)_5(OH)_6(CO_3)_2$, was observed in the unpromoted binary Cu/ZnO system. Toward intermediate promoter concentrations, the relative crystalline fraction of the byproduct phases decreased at the expense of zM, which was the only crystalline precursor phase detected by PXRD for [Al] = 3.3 and 4%. Despite the fact that smaller Cu particles typically evolve from aurichalcite[27] and hydrotalcite,[30] they can be regarded as undesired precursor phases because their mesostructure gives rise to encapsulation of Cu particles in large oxide aggregates, making them inaccessible.

Careful analysis of the PXRD patterns revealed variations in the crystal structure of zM with [Al]. In particular, the $d_{20\bar{1}}$ spacing of the zM unit cell contracted with decreasing [Al] below 13% (Figure 2a, open symbols; also see Figure S2 in the Supporting Information), and a sharp minimum in the $d_{20\bar{1}}$ spacing was observed for [Al] = 3.3%. The lattice contraction in this direction is caused by the substitution of Jahn−Teller-elongated octahedral CuO_6 building units with non-Jahn−Teller-elongated ZnO_6 units.[17,31] Thus, the Cu^{2+} concentration in zM, which in phase mixtures of different copper(II)/zinc hydroxycarbonates is otherwise hard to measure accurately, could be indirectly determined by PXRD. The results showed that variation of [Al] in the starting solution has a direct influence of the concentration of Cu^{2+} ions in zM. It can be concluded that low amounts of Al promote the incorporation of Zn into zM by affecting the phase formation of the precursor system during aging of the coprecipitate. For [Al] near 3−4%, the formation of crystalline Zn-rich byproduct phases

dx.doi.org/10.1021/ja310456f | J. Am. Chem. Soc. 2013, 135, 6061−6068

(aurichalcite, hydrotalcite) is effectively hindered, resulting in the desired preferential incorporation of Zn ions into zM.

This phase composition-directing effect, however, cannot explain the lower value of $d_{20\bar{1}}$ at [Al] = 3.3% relative to the sample [Al] = 4%, which also consists of phase-pure zM. A likely explanation for the significantly higher substitution of Cu^{2+} in the former sample is direct coincorporation of Zn^{2+} and Al^{3+} ions into the zM precursor. Non-Jahn−Teller-distorted AlO_6 units can further contribute to the dilution of Cu^{2+} by Zn^{2+}/Al^{3+} in the zM lattice and lead to an additional sharp decrease in $d_{20\bar{1}}$ due the significantly smaller ionic radius of Al^{3+}.

To test whether the malachite structure is indeed able to incorporate small amounts of Al^{3+}, substitution experiments in the binary Zn-free Cu/Al system were conducted. Indeed, a contraction of $d_{20\bar{1}}$ with increasing Al content was observed (Figure S5 in the Supporting Information), clearly indicating the presence of non-Jahn−Teller ions in the lattice, an effect that in the absence of Zn^{2+} can be explained only by incorporation of Al^{3+} into the malachite lattice. The observed unit cell contraction indicates Al^{3+} incorporation into Zn-free malachite up to approximately 3%. Thus, the maximal Al^{3+} incorporation that can be tolerated by the malachite structure is much lower than that for Zn^{2+} (up to approximately 28%[31]). This is obviously due to the excess positive charge induced by Al^{3+} residing on Cu^{2+} sites. Possible mechanisms of charge compensation include the formation of cation or proton vacancies in the malachite lattice or local changes in the connectivity pattern of the building blocks.

The high degree of Cu^{2+} substitution in the catalyst precursor containing 3.3% Al can therefore be explained by the simultaneous coincorporation of Zn^{2+} and Al^{3+} in this compositional window, while at 4% the Al^{3+} concentration is high enough to trigger the segregation of Al-rich byproduct phases and Al^{3+} depletion from zM.

On the basis of these considerations, the critical influence of the Al promoter during the early stages of catalyst preparation can be summarized as follows: High concentrations—as often applied in industrial synthesis—lead to crystallization of Al-rich hydrotalcite-like material that also incorporates large amounts of Zn, which in turn is not available as a diluent for Cu^{2+} in the zM structure and later as ZnO stabilizer in the highly active zM-derived domains in the final catalyst (see Figure 1). Lowering [Al] decreases the chemical potential of Al (μ_{Al}) in the coprecipitate slurry during phase formation of the precursor. At [Al] = 4%, μ_{Al} is too low for formation of hydrotalcite, and more Zn becomes available for incorporation into zM, causing a gradual increase in the zM fraction and a decrease in $d_{20\bar{1}}$. At this point, Al is probably precipitated in the form of undetected finely dispersed $Al(OH)_3$, which acts as a "sink" for Al^{3+}. Upon a further decrease in [Al] to 3.3%, incorporation of Al^{3+} itself into zM in addition to Zn^{2+} becomes possible because the concentration of Al^{3+} is now low enough to allow the malachite parent structure to compensate for the excess charge by a defect mechanism.

Formation of a segregated Al storage phase such as $Al(OH)_3$ becomes disfavored. This window of μ_{Al} is rather narrow, and for too low Al concentrations the system evolves toward the binary boundary case as the amount of Al^{3+} becomes limiting for incorporation into zM. It can be concluded that at a given industrially relevant Cu:Zn ratio of 70:30, it is possible to incorporate all of the metal species, including all of the Zn and the Al promoter, into a single substituted malachite precursor phase at Al concentrations up to 3.3%. This phase-pure Al-doped zM precursor exhibits a perfect atomic distribution of all three metal species and enables the evolution of a uniform high-performance catalyst with high dispersion of all of the constituent phases (active Cu metal, ZnO stabilizer, and Al_2O_3 promoter), which is the "secret" of the industrial catalyst synthesis for effective promoter incorporation.

The importance of these considerations for the activity of the final catalyst is apparent from Figure 2a, which shows an inverse relationship between $d_{20\bar{1}}$ of the zM precursor and the catalytic activity of the resulting catalyst in methanol synthesis. This precursor structure−performance relationship confirms that zM is the relevant precursor phase for highly active catalysts, and furthermore, comparative characterization this series of samples can be used to shed light on the role of the Al promoter in the final catalyst.

Above, the Al concentration in the starting solution was identified as a critical parameter to influence the incorporation of both Zn^{2+} and Al^{3+} in zM. This coincorporation results in an atomically uniform distribution in the precursor and in a very homogeneous element distribution after calcination and reduction, stabilizing Cu with high dispersion in the final catalyst. Thus, the geometric effect of dilution of Cu^{2+} on an atomic level in the precursor phase by Zn^{2+} and Al^{3+} is one explanation for the promoting effect of Al in this system. As a result of this structural promotion, however, one would expect an increase in exposed Cu surface area (SA_{Cu}) and a more or less constant intrinsic (i.e., SA_{Cu}-normalized) activity with increasing substitution (decreasing $d_{20\bar{1}}$). SA_{Cu} was measured for the series of catalysts using N_2O reactive frontal chromatography,[32,33] and the intrinsic activities were calculated (Figure 2c). It can be seen that there is a significant decrease in intrinsic activity with increasing [Al]. The unpromoted binary sample, despite being the poorest catalyst on the absolute scale, shows the highest intrinsic activity of the sample series, which is a result of the by-far lowest SA_{Cu} for this sample. For the promoted catalysts, which possess similar and much higher SA_{Cu}, the intrinsic activity is high at low Al content, decreases until [Al] reaches approximately 6.5%, and then shows a slight increase again into the regime of conventional catalyst composition.

Interestingly, the relatively Al-poor catalysts with [Al] = 2.5 and 3.3% successfully combine a high SA_{Cu} with a relatively high intrinsic activity. Their low Al:Zn ratios of <10% approach the compositional range where Al doping of ZnO with Al residing on the tetrahedral Zn sites in the ZnO wurzite-type lattice has been reported.[34,35] It is thus tempting to relate the promotion of the intrinsic activity of Cu to Al doping of the ZnO component in the final catalyst.

Such doping is facilitated when Al is atomically distributed in the single-phase zM precursor, as in the most active sample having [Al] = 3.3%. Solid-state ^{27}Al MAS NMR spectroscopy was applied to investigate the local environment of Al^{3+} in selected $Cu/ZnO/Al_2O_3$ catalysts after reduction. In Figure 3a, the intensity-normalized NMR spectra are compared with that of a coprecipitated Cu-free, Al-doped ZnO model material (Zn:Al = 97:3[35]). The NMR spectra of the $Cu/ZnO/Al_2O_3$ catalysts are dominated by an asymmetric peak centered between 65 and 70 ppm independent of the Al content. The signal is very broad, suggesting the presence of several Al species with a varying degree of defect concentrations, which causes a distribution of quadrupolar coupling constants. While probably the main contribution is caused by Al^{3+} tetrahedrally coordinated by oxygen, fivefold and octahedrally coordinated Al

dx.doi.org/10.1021/ja310456f | J. Am. Chem. Soc. 2013, 135, 6061−6068

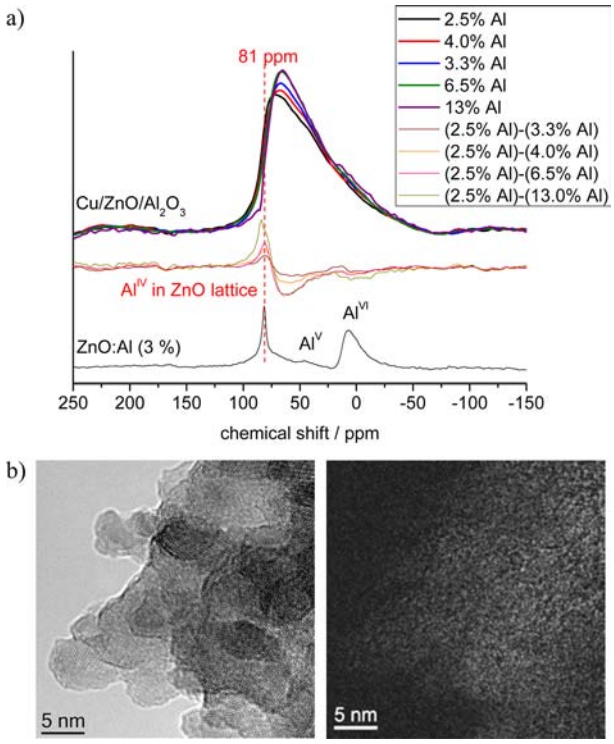

Figure 3. (a) ^{27}Al MAS NMR spectra of reduced $Cu/ZnO/Al_2O_3$ catalysts with different Al contents and their difference spectra. All of the spectra were normalized to equal intensity to highlight changes in the spectral shape. The bottom curve shows the spectrum of a ZnO:Al sample with an Al content of 3 mol % taken from literature.[35] (b) (left) High-resolution transmission electron microscopy image of the calcined $CuO/ZnO/Al_2O_3$ catalyst with an Al content of 3.3% showing crystalline CuO and ZnO nanoparticles and (right) the corresponding Al map, which shows good dispersion and a homogeneous distribution of the Al species.

ions also seem to be present. No clear assignment of the spectra to any alumina bulk reference phase was possible, which can be explained by the nanostructured nature of the catalyst and the uniform distribution of Al, as shown in Figure 3b for the best-promoted calcined catalyst with [Al] = 3.3%.

However, systematic trends become apparent in the difference plots of the spectra, which reveal strong and relatively narrow deviations in the spectral region around 81 ppm (Figure 3a). These might be explained by differences in the degree of disorder that could cause changes in the line profiles, but the difference signal coincides precisely with the signal reported for tetrahedrally coordinated Al^{3+} residing on the Zn^{2+} sites of the ZnO in the ZnO lattice (Al_{Zn}),[34,36] suggesting that a varying fraction of the Al promoter in the $Cu/ZnO/Al_2O_3$ catalyst is present as a dopant in the ZnO stabilizer component. This fraction of Al in ZnO:Al is estimated to be low in comparison to the total amount of Al, but interestingly, it increases monotonically as the concentration of Al in the catalyst decreases and shows a correlation with the intrinsic activity. Thus, the sample with the lowest [Al] (2.5%) shows the highest relative amount of Al_{Zn} and the highest intrinsic activity among the promoted catalysts. However, the structural trends of the zM precursor discussed above suggest that the absolute amount of Al_{Zn} is probably highest for the most active catalyst ([Al] = 3.3%), which exhibits the lowest $d_{20\bar{1}}$ because of the highest coincorporation of Al in the Cu/Zn precursor.

As a further test of whether promoter species are incorporated into the zincite lattice in the catalysts, Al^{3+} was substituted with Ga^{3+} and an analogous series of $Cu/ZnO/Ga_2O_3$ samples was prepared in the interesting range of $0\% \leq [Ga] \leq 3\%$. Despite the larger ionic radius, Ga^{3+} exhibits properties in aqueous solution and solid-state compounds that are similar to those of Al^{3+} and can serve as a proxy for the promoter, enabling further investigation by K-edge absorption spectroscopy using hard X-rays, which is well-suited for determination of the Ga speciation.[37]

The Ga K-edge XANES spectra of a calcined $CuO/ZnO/Ga_2O_3$ catalyst containing 3% Ga and selected reference materials are shown in Figure 4 (for details, see Figure S6 in

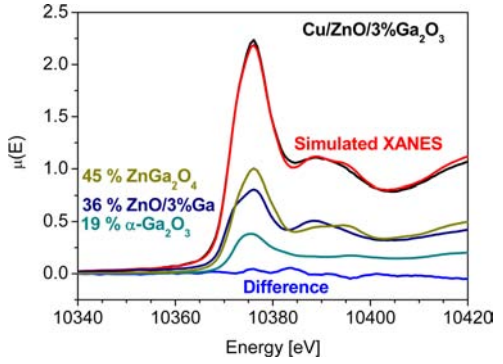

Figure 4. Ga K-edge XANES spectra of the calcined $CuO/ZnO/Ga_2O_3$ catalyst with a Ga content of 3 mol % and results of the linear-combination fit using the experimental spectra of the indicated gallium oxide reference materials.

the Supporting Information). A fit of the experimental spectrum of the Ga-promoted catalyst as a linear combination of the reference spectra required three phases, $ZnGa_2O_4$, α-Ga_2O_3, and ZnO:3%Ga. This result confirmed the picture already seen in the ^{27}Al NMR results for the Al-promoted sample: a variety of gallium oxide species were present in the catalyst, among which Ga doped into ZnO could be clearly identified. It is noted that no satisfying fit was possible without the reference spectrum of ZnO:Ga, thus providing support for the presence of significant amounts of Ga^{3+} as Ga_{Zn} in ZnO in the promoted catalysts (Table S1 and Figure S6 in the Supporting Information).

Interestingly, the inverse trends in $d_{20\bar{1}}$ and catalytic activity with promoter concentration previously observed for the Al promoter were also found for the Ga series, suggesting that these correlations represent a general concept for the promotion of Cu/ZnO catalysts. Cr-promoted samples were also prepared analogously, and the same trend was observed but to a lesser extent. Cr^{3+} exhibits an ionic radius similar to that of Ga^{3+}, and these ions together with Al^{3+} form a family of dopants that promote the n-type semiconductivity of ZnO.[38]

These results reveal that in addition to the geometric effect, a second type of electronic promotion effect is present. It contributes to the modification of the ZnO component by partial substitution of Zn^{2+} with Al^{3+} (or Ga^{3+} or Cr^{3+}). Such a substitution strongly affects the defect chemistry and redox properties as well the electronic structure and electrical conductivity[39] of ZnO, which can be related to the intrinsic activity of the Cu/ZnO catalyst as discussed below.

Despite the fact that even at very low promoter content only a fraction of the promoter is responsible for this effect, the

dx.doi.org/10.1021/ja310456f | J. Am. Chem. Soc. 2013, 135, 6061−6068

structure−performance relationship shown in Figure 2 allows this relevant fraction of the promoter to be tracked back to the amount of promoter initially incorporated into the lattice of the zM precursor phase. Although deconvolution of the two promoting effects should be nontrivial, a simple linear correlation of catalytic activity and the degree of substitution in the zM precursor lattice (as indicated by the contraction of the $d_{20\bar{1}}$ spacing) was observed for the $Cu/ZnO/Al_2O_3$, $Cu/ZnO/Ga_2O_3$, and $Cu/ZnO/Cr_2O_3$ catalysts (Figure 5). The

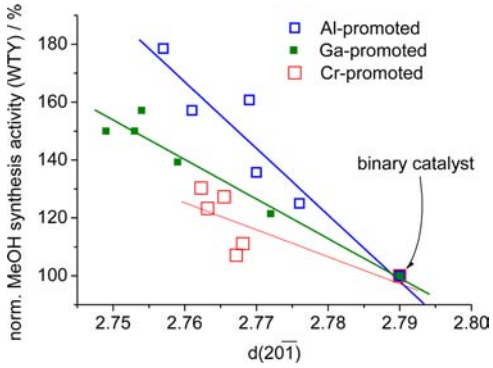

Figure 5. Linear correlations of the catalytic performance of the final catalyst and the d spacing of the $20\bar{1}$ planes in the zM precursor for the promoter series with Al, Ga, and Cr.

different slopes for the various catalyst families suggest that Al is a more efficient promoter than Ga and that Cr is the least effective, while the mechanism of promotion and promoter incorporation is the same.

An early report on the effect of electronic modification of semiconductor supports for a metal-catalyzed reaction was given by Schwab et al.[40] They studied dehydration of formic acid on different metals (Ni, Co, Ag) and observed an increase in activation energy with increasing conductivity of the Al_2O_3 support, which they tuned by doping with other oxides. This was interpreted as a result of the band-bending effect at the metal−semiconductor interface (Schottky barrier), a concept later also proposed to be relevant for methanol synthesis on metal/semiconductor catalysts by Frost.[41]

For Cu/ZnO-based catalysts, at present there is agreement in the literature that the Cu−ZnO interface plays an important role in the methanol synthesis activity, and several models for the active sites involving the so-called Cu−ZnO synergy[42−44] have been suggested. A dynamic strong metal−support interaction (SMSI) has been observed at a model interface contact of a Cu nanoparticle and a crystalline ZnO surface[45−47] that can explain the effects observed in this work. As a result of SMSI, Cu particles are deformed,[48] and ZnO_x ($x < 1$) moieties are formed under reducing conditions at the Cu−ZnO interface and migrate onto the metal surface. This in situ-formed decorated surface is suggested to hold the active sites for methanol synthesis. Here the reducibility of ZnO is a critical factor, as oxygen vacancies play an important role in such dynamic behavior.[47] Hence, such an effect is expected to be strongly affected by changes in the ZnO component due to Al^{3+} incorporation, serving as an explanation for the electronic promotion of Cu/ZnO by Al.

Accordingly, when Mg^{2+} was used as an additive to the Cu/ZnO catalyst following the same synthesis concept, no electronic promotion of the methanol synthesis activity was observed. Instead, Mg had a detrimental effect on the intrinsic activity. This observation is well in line with the critical role of the support reducibility. Mg^{2+} and Zn^{2+} do not exhibit a charge mismatch that needs to be compensated by defects in the sublattices of ZnO. Moreover, Mg^{2+} is known to make ZnO "more ionic" and to widen the band gap in MgO−ZnO solid solutions.[38] Thus, lower reducibility and a negative effect on SMSI can be expected. A comparison of the roles of different promoters is given in Figure 6. Figure 6c shows that all of the

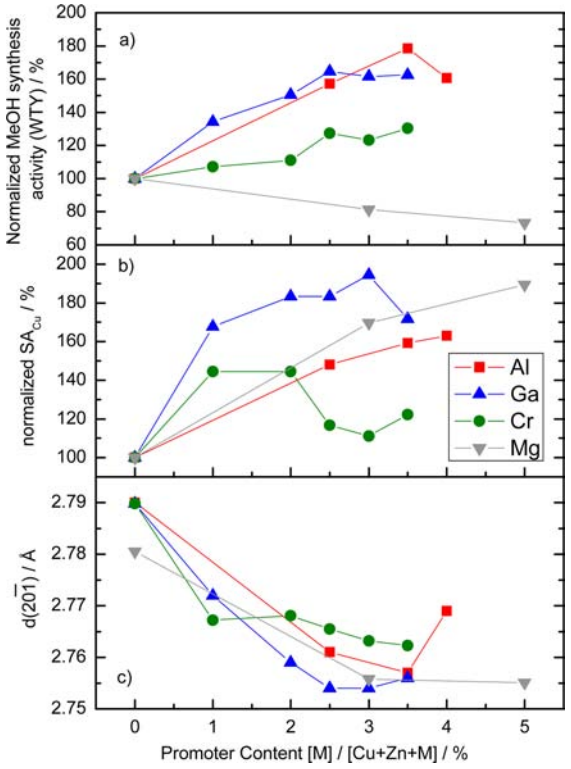

Figure 6. Overview of the promoting effects of Al_2O_3, Ga_2O_3, Cr_2O_3, and MgO on Cu/ZnO catalysts: (a) methanol synthesis activity relative to the unpromoted catalyst as a result of structural and electronic promotion; (b) SA_{Cu} relative to the unpromoted catalyst as a result of structural promotion; (c) effect of the promoter on $d_{20\bar{1}}$ of the zM precursor.

additives have a contracting effect on $d_{20\bar{1}}$ when used at low concentrations, indicating incorporation into the zM lattice. Related to this incorporation, a structural promotion effect was observed in all cases, as shown by the increase in SA_{Cu} (Figure 6b). This effect is least obvious for Cr but clearly visible for Mg, which should be easier to incorporate into the precursor as no charge mismatch occurs upon substitution. The electronic promotion effect is seen in Figure 6a. It is observed only for those promoters that create donor levels and enhance the n-type semiconductivity of ZnO and is not present for Mg.

We have recently shown that the high activity of industrial catalysts can be explained by a combination of a static defect model and the dynamic SMSI effect: dynamic surface coverage of ZnO_x was observed while the Cu particles maintained their defect structure.[49] Thus, a highly active catalyst requires both a defective Cu surface with high-energy sites and the presence of Zn at the surface, which is supplied by partial reduction of ZnO. As a result of the present study, potential tuning of this latter effect by modification of the properties of ZnO is proposed[35] as the origin of catalyst promotion with Al.

dx.doi.org/10.1021/ja310456f | J. Am. Chem. Soc. 2013, 135, 6061−6068

While the structural promotion effect on the Cu dispersion is rather unique to the role of the zM precursor for Cu/ZnO/Al_2O_3 catalysts, this latter electronic effect is a mode of operation of catalyst promoters that also has potential relevance to many other metal/oxide catalysts, where SMSI has been observed to have a beneficial effect on the catalytic properties. The degree of surface coverage by oxide entities under a given chemical potential of the catalytic reaction depends on the reducibility of the oxide support, and the results of this study suggest that this latter property can tuned by promoter-induced defects to adjust the correct degree of surface coverage for in situ formation of active sites.

CONCLUSIONS

In summary, it has been shown that industrial Cu/ZnO/Al_2O_3 catalysts—if correctly promoted—should instead be written as Cu/ZnO:Al. The effect of the Al promoter is multifold: First, it affects phase formation of the precursor in the early stage of preparation during crystallization of the coprecipitate. The chemical potential of Al in the precursor slurry, which can be easily controlled by the concentration of Al^{3+} in the starting solution, determines the desired incorporation of Zn^{2+} as well as Al^{3+} itself into the catalyst precursor and promotes the dispersion of Cu in the final catalyst by a geometric effect. This structural promotion can also be achieved by addition of Ga, Cr, or Mg following the same mechanism via incorporation into the cationic lattice of the precursor.

Second, the presence of Al also influences the intrinsic activity of the Cu(0) surface. For intrinsically more active samples, a larger fraction of Al^{3+} was found to reside on the Zn^{2+} sites in the ZnO component, and analogous behavior was observed for Ga_2O_3- and Cr_2O_3-promoted Cu/ZnO catalysts, all of which improve the n-type semiconductivity of ZnO. In addition to the structural effect, an electronic promotion effect is also operational in industrial methanol synthesis catalysts: modification of the defect chemistry and reducibility of ZnO by incorporation of Al^{3+} (or Ga^{3+} or Cr^{3+}) affects the catalytically active Cu surface by dynamical strong metal support interaction—an observation that opens the door for rational promotion of other metal/oxide catalysts with reducible supports as well. Accordingly, making the ZnO support less reducible by Mg incorporation was found to have a detrimental effect on the activity.

Within the present study, the performance of a Cu/ZnO-based methanol synthesis catalyst was increased by approximately 80% relative to the unpromoted catalyst and about 40% relative to a state-of-the-art catalyst formulation as a result of improved Al promotion by more effective promoter incorporation.

ASSOCIATED CONTENT

Supporting Information

Experimental details of syntheses, XRD and TGA data, and XANES fitting results. This material is available free of charge via the Internet at http://pubs.acs.org.

AUTHOR INFORMATION

Corresponding Author

behrens@fhi-berlin.mpg.de

Notes

The authors declare no competing financial interest.

ACKNOWLEDGMENTS

Financial support was provided by the German Federal Ministry of Education and Research (BMBF, FKZ 01RI0529), the Bayerisches Wissenschaftsministerium (NW-0810-0002), and Clariant Produkte (Deutschland) GmbH. We thank Igor Kasatkin, Thomas Hansen, Frank Girgsdies, Steffi Kühl, Giulio Lolli, Nelli Muratova, and Edith Kitzelmann for their help with sample characterizations and Liandi Li and Antje Ota for preparation of gallium oxide reference materials. HASYLAB at DESY (Hamburg, Germany) is acknowledged for allocation of beamtime. Martin Muhler and Annette Trunschke are acknowledged for fruitful discussions.

REFERENCES

(1) Hutchings, G. J. *Catal. Lett.* **2001**, *75*, 1.
(2) Koel, B. E.; Kim, J. In *Handbook of Heterogeneous Catalysis*; Ertl, G., Knözinger, H., Schüth, F.; Weitkamp, J., Eds.; Wiley-VCH: Weinheim, Germany, 2008; pp 1593−1624.
(3) Campbell, C. T.; Grant, A. W.; Starr, D. E.; Parker, S. C.; Bondzie, V. A. *Top. Catal.* **2000**, *14*, 43.
(4) Nilius, N.; Risse, T.; Schauermann, S.; Shaikhutdinov, S.; Sterrer, M.; Freund, H.-J. *Top. Catal.* **2011**, *54*, 4.
(5) Vayssilov, G. N.; Lykhach, Y.; Migani, A.; Staudt, T.; Petrova, G. P.; Tsud, N.; Skala, T.; Bruix, A.; Illas, F.; Prince, K. C.; Matolin, V.; Neyman, K. M.; Libuda, J. *Nat. Mater.* **2011**, *10*, 310.
(6) Bengaard, H. S.; Alstrup, I.; Chorkendorff, I.; Ullmann, S.; Rostrup-Nielsen, J. R.; Nørskov, J. K. *J. Catal.* **1999**, *187*, 238.
(7) Ertl, G.; Lee, S. B.; Weiss, M. *Surf. Sci.* **1982**, *114*, 527.
(8) Nakamura, J.; Campbell, J. M.; Campbell, C. T. *J. Chem. Soc., Faraday Trans.* **1990**, *86*, 2725.
(9) Natesakhawat, S.; Lekse, J. W.; Baltrus, J. P.; Ohodnicki, P. R.; Howard, B. H.; Deng, X.; Matranga, C. *ACS Catal.* **2012**, *2*, 1667.
(10) Słoczynski, J.; Grabowski, R.; Olszewski, P.; Kozłowska, A.; Stoch, J.; Lachowska, M.; Skrzypek, J. *Appl. Catal., A* **2006**, *310*, 127.
(11) Olah, G. A.; Goeppert, A.; Prakash, G. K. S. *J. Org. Chem.* **2009**, *74*, 487.
(12) Schlögl, R. *ChemSusChem* **2010**, *3*, 209.
(13) Rihko-Struckmann, L. K.; Peschel, A.; Hanke-Rauschenbach, R.; Sundmacher, K. *Ind. Eng. Chem. Res.* **2010**, *49*, 11073.
(14) Hansen, J. B.; Højlund Nielsen, P. E. In *Handbook of Heterogenous Catalysis*; Ertl, G., Knözinger, H., Schüth, F., Weitkamp, J., Eds.; Wiley-VCH: Weinheim, Germany, 2008; pp 2920−2949.
(15) Günter, M. M.; Ressler, T.; Bems, B.; Büscher, C.; Genger, T.; Hinrichsen, O.; Muhler, M.; Schlögl, R. *Catal. Lett.* **2001**, *71*, 37.
(16) Kasatkin, I.; Kurr, P.; Kniep, B.; Trunschke, A.; Schlögl, R. *Angew. Chem.* **2007**, *119*, 7465.
(17) Behrens, M. *J. Catal.* **2009**, *267*, 24.
(18) Baltes, C.; Vukojevic, S.; Schüth, F. *J. Catal.* **2008**, *258*, 334.
(19) Couves, J. W.; Thomas, J. M.; Waller, D.; Jones, R. H.; Dentt, A.; Derbyshire, G. E.; Greaves, G. N. *Nature* **1991**, *354*, 465.
(20) Waller, D.; Stirling, D.; Stone, F. S.; Spencer, M. S. *Faraday Discuss. Chem. Soc.* **1989**, *87*, 107.
(21) Twigg, M. V.; Spencer, M. S. *Top. Catal.* **2003**, *22*, 191.
(22) Kurtz, M.; Bauer, N.; Büscher, C.; Wilmer, H.; Hinrichsen, O.; Becker, R.; Rabe, S.; Merz, K.; Driess, M.; Fischer, R. A.; Muhler, M. *Catal. Lett.* **2004**, *92*, 49.
(23) Saito, M.; Murata, K. *Catal. Surv. Asia* **2004**, *8*, 285.
(24) Coelho, A. A. *TOPAS: General Profile and Structure Analysis Software for Powder Diffraction Data*, version 3.0; Bruker AXS GmbH: Karlsruhe, Germany, 2006.
(25) Zhang, S.; Wu, X.; Mehring, M. *Chem. Phys. Lett.* **1990**, *173*, 481.
(26) Fiedler, E.; Grossmann, G.; Kersebohm, D. B.; Weiss, G.; Witte, C. In *Ullmann's Encyclopedia of Industrial Chemistry*; Wiley-VCH: Weinheim, Germany, 2011; Vol. 23, pp 25−48.

(27) Whittle, D. M.; Mirzaei, A. A.; Hargreaves, J. S. J.; Joyner, R. W.; Kiely, C. J.; Taylor, S. H.; Hutchings, G. J. *Phys. Chem. Chem. Phys.* **2002**, *4*, 5915.
(28) Millar, G. J.; Holm, I. H.; Uwins, P. J. R.; Drennan, J. *J. Chem. Soc., Faraday Trans.* **1998**, *94*, 593.
(29) Behrens, M.; Brennecke, D.; Girgsdies, F.; Kißner, S.; Trunschke, A.; Nasrudin, N.; Zakaria, S.; Idris, N. F.; Abd Hamid, S. B.; Kniep, B.; Fischer, R.; Busser, W.; Muhler, M.; Schlögl, R. *Appl. Catal., A* **2011**, *392*, 93.
(30) Behrens, M.; Kasatkin, I.; Kühl, S.; Weinberg, G. *Chem. Mater.* **2010**, *22*, 386.
(31) Behrens, M.; Girgsdies, F. *Z. Anorg. Allg. Chem.* **2010**, *636*, 919.
(32) Chinchen, G. C.; Hay, C. M.; Vanderwell, H. D.; Waugh, K. C. *J. Catal.* **1987**, *103*, 79.
(33) Hinrichsen, O.; Genger, T.; Muhler, M. *Chem. Eng. Technol.* **2000**, *23*, 956.
(34) Miao, S.; Naumann d'Alnoncourt, R.; Reinecke, T.; Kasatkin, I.; Behrens, M.; Schlögl, R.; Muhler, M. *Eur. J. Inorg. Chem.* **2009**, 910.
(35) Behrens, M.; Lolli, G.; Muratova, N.; Kasatkin, I.; Hävecker, M.; Naumann d'Alnoncourt, R.; Storcheva, O.; Köhler, K.; Muhler, M.; Schlögl, R. *Phys. Chem. Chem. Phys.* **2013**, *15*, 1374.
(36) Avadhut, Y. S.; Weber, J.; Hammarberg, E.; Feldmann, C.; Schmedt auf der Günne, J. *Phys. Chem. Chem. Phys.* **2012**, *14*, 11610.
(37) Nishi, K.; Shimizu, K.-I.; Takamatsu, M.; Yoshida, H.; Satsuma, A.; Tanaka, T.; Yoshida, S.; Hattori, T. *J. Phys. Chem. B* **1998**, *102*, 10190.
(38) Janotti, A.; Van de Walle, C. G. *Rep. Prog. Phys.* **2009**, *72*, 126501.
(39) Wang, R.; Sleight, A. W.; Cleary, D. *Chem. Mater.* **2011**, *8*, 433.
(40) Schwab, G.-M.; Block, J.; Schultze, D. *Angew. Chem.* **1959**, *71*, 101.
(41) Frost, J. C. *Nature* **1988**, *334*, 577.
(42) Burch, R.; Golunski, S. E.; Spencer, M. S. *J. Chem. Soc., Faraday Trans.* **1990**, *28*, 2683.
(43) Nakamura, J.; Choi, Y.; Fujitani, T. *Top. Catal.* **2003**, *22*, 277.
(44) Frost, J. C. *Nature* **1988**, *334*, 577.
(45) Topsøe, N.-Y.; Topsøe, H. *Top. Catal.* **1999**, *8*, 267.
(46) Hansen, P. L.; Wagner, J. B.; Helveg, S.; Rostrup-Nielsen, J. R.; Clausen, B. S.; Topsøe, H. *Science* **2002**, *295*, 2053.
(47) Grunwaldt, J.-D.; Molenbroek, A. M.; Topsøe, N.-Y.; Topsøe, H.; Clausen, B. S. *J. Catal.* **2000**, *194*, 452.
(48) Vesborg, P. C. K.; Chorkendorff, I.; Knudsen, I.; Balmes, O.; Nerlov, J.; Molenbroek, A. M.; Clausen, B. S.; Helveg, S. *J. Catal.* **2009**, *262*, 65.
(49) Behrens, M.; Studt, F.; Kasatkin, I.; Kühl, S.; Hävecker, M.; Abild-Pedersen, F.; Zander, S.; Girgsdies, F.; Kurr, P.; Kniep, B.; Tovar, M.; Fischer, R. W.; Nørskov, J. K.; Schlögl, R. *Science* **2012**, *336*, 893.